Study of Unsteady Surface Pressure on a Turret via Pressure-Sensitive Paint

Kyle Hird[1], Thomas J. Juliano[2], James W. Gregory[3]
The Ohio State University, Columbus, Ohio 43235

Stanislav Gordeyev[4], Nicholas De Lucca[5], Eric Jumper[6]
University of Notre Dame, Notre Dame, Indiana 46545

James Thordahl[7] and Donald J. Wittich[8]
Air Force Research Laboratory, Directed Energy Directorate, Kirtland AFB, NM 87117

Fast-response pressure-sensitive paint (PSP) was used in this work for a study of the unsteady surface pressures resulting from the complex separated flow over a hemispherical turret model. The turret includes several distinct features such as a flat window and crevices that are based on functional requirements, but also introduce interesting additional compact unsteady flow features. Three high-speed cameras imaged the paint luminescence at 2 kHz, producing pressure time histories over the entire model. These pressure data were integrated over the model surface in order to determine unsteady loads. Fast-response PSP successfully resolved very small pressure features that had aperiodic fluctuations of at least several kilohertz.

I.   Introduction

In this study, a pressure-sensitive paint (PSP) formula based on platinum porphyrin with a porous base layer was employed to measure the spatially and temporally varying pressure over the surface of a realistic hemisphere-on-cylinder turret with either a flat or a conformal aperture at various geometric configurations at subsonic speeds. The objective of the study is to yield insight into the complex unsteady fluid dynamics of the turret's separated wake, and the interaction of this wake with the turret model (a fluid-structure interaction problem). Multiple high-speed cameras were used in an effort to record time-resolved pressures over the entire three-dimensional surface of this turret model. This rich data set may be integrated over the model surface in order to determine unsteady loading, and to identify the specific pressure features that drive the frequency and magnitude of the loads.

Pressure-sensitive paint is an optical method for measuring surface pressures.[1,2] It is based on oxygen quenching of excited-state luminescence of a painted model. The intensity of the emitted light from the model is inversely proportional to the local partial pressure of oxygen, and due to Henry's law, pressure. The distinct advantages of

---

[1] Undergraduate Research Assistant, Department of Mechanical and Aerospace Engineering, 2300 West Case Rd.

[2] Postdoctoral Research Associate, Department of Mechanical and Aerospace Engineering, 2300 West Case Rd., AIAA Member. Currently NRC Postdoctoral Research Fellow at Air Force Research Laboratory, Wright-Patterson AFB, OH.

[3] Assistant Professor, Department of Mechanical and Aerospace Engineering, 2300 West Case Rd., AIAA Senior Member.

[4] Research Associate Professor, Department of Aerospace and Mechanical Engineering, Hessert Laboratory for Aerospace Research, AIAA Associate Fellow.

[5] Graduate Student, Department of Aerospace and Mechanical Engineering, Hessert Laboratory for Aerospace Research, AIAA Student Member.

[6] Professor, Department of Mechanical and Aerospace Engineering, Hessert Laboratory for Aerospace Research, Notre Dame, IN 46556, AIAA Fellow.

[7] Sr. Project Engineer, The Aerospace Corporation, 2155 Louisiana Blvd, Suite 5000, Albuquerque, NM 87110.

[8] Aerospace Engineer, Laser Division, 3550 Aberdeen Ave SE.

PSP are that it offers very high spatial resolution at relatively low cost. Until recently, PSP has been predominantly limited to steady-state pressure measurements due to the slow frequency response of the paint. The response time is primarily governed by the paint thickness and the diffusivity of the paint binder.[3,4] Recently, however, porous PSP formulations have been developed which greatly enhance the binder's diffusivity, resulting in frequency response on the order of 6 kHz.[3-6] In some paint formulations, the frequency response is actually now limited by the luminophore lifetime rather than the binder gas diffusion characteristics.[3,5,7]

The specific PSP formulation used in this work is a polymer-ceramic binder with platinum tetra(pentafluorophenyl) porphyrin (PtTFPP) as a luminophore. This PSP is known to have high frequency response (~6 kHz,[3-7] as shown in Figure 1) and is very bright due to the use of large amounts of titanium dioxide in the binder layer. These two characteristics make it well-suited for high-speed imaging of transient phenomena. Furthermore, the sensitivity of the paint is high enough such that it has been used for measuring acoustic-level pressure fluctuations.[8,9] The polymer-ceramic/PtTFPP paint formulation has been used recently for study of flow over a hemispherical dome in a manner similar to the current work.[10,11] Fang et al.[10] resolved the unsteady shock and separation behavior on a dome using phase-averaging techniques. In more recent work, Fang et al.[11] performed a comparative study between three leading data acquisition techniques (phase averaging, single-shot lifetime, and high-speed imaging), and found that time-resolved techniques without any cycle averaging were required to accurately measure the transient phenomena that were present on the hemispherical dome. This led to the selection of high-speed imaging for the current work.
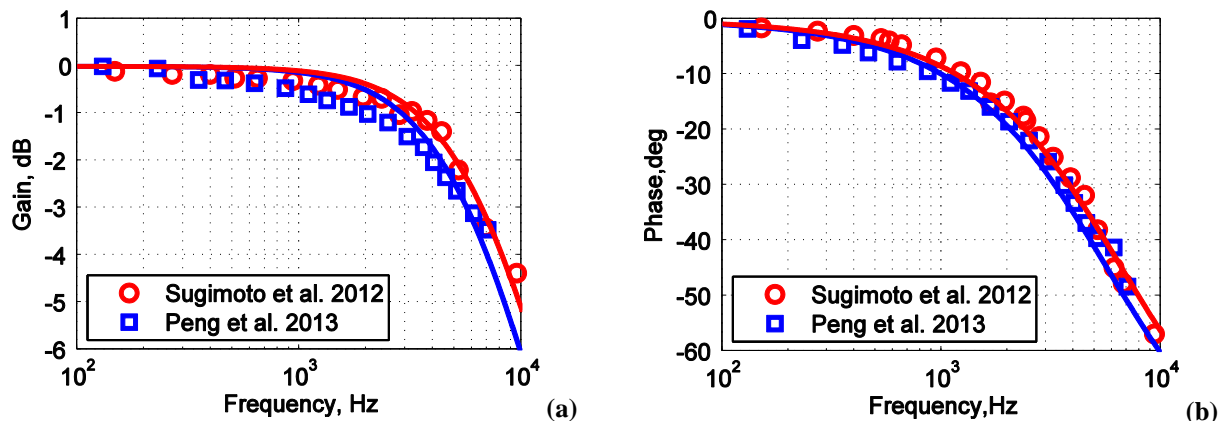

Figure 1: Dynamic response of polymer/ceramic PSP with PtTFPP with (a) magnitude and (b) phase response. Both independent sets of calibration data, each performed in an acoustic resonance tube, indicate a -3dB roll-off point at 6 kHz.[5,6]

Low-noise, high-speed cameras are being used for an increasing number of unsteady PSP investigations. Since high-speed imaging results in such a large volume of spatially- and temporally-resolved data, there has been a concomitant development of image processing techniques for extracting relevant flow features. Nakakita employed high-speed imaging to study the flow over a two-dimensional circular cylinder in crossflow.[12] A separate power spectrum was computed for each pixel in the image (i.e., virtual pressure tap). The amplitude of the pressure fluctuations in each frequency band yielded insight into the spatial structure and relative phase of the pressure fluctuations. In a separate investigation, Nakakita studied the generation of trailing edge noise from a 2D airfoil section using a traversing point measurement (laser and photomultiplier tube instrumentation) and high-speed imaging, with good agreement. Both the circular cylinder work[12] and the airfoil work[13] done by Nakakita were conducted at fairly low speed (~ 30 m/s in a small-scale wind tunnel). Crafton et al. performed high-speed imaging of the surface pressure field below the interaction of a transverse jet in supersonic crossflow.[14] They decomposed the signal into contour plots of energy in several spectral bands for visualization of the spectral content of various flow structures (bow shock, expansion fans, horseshoe vortex, etc.). They also performed cross-correlations of pressure measurements at various spatial locations in order to infer causal mechanisms. Nakakita et al. recently used high-speed imaging of fast PSP to study shock/boundary-layer interaction on a rocket fairing in transonic flow, with spectral analysis revealing the shock structure and oscillation width.[15] In separate investigations, Nakakita and Arizono[16] and Mérienne et al.[17] studied transonic buffet on models of a commercial transport wing. Both investigations clearly resolved the unsteady movement of the complex shock structure on the wing. The work of

2

American Institute of Aeronautics and Astronautics

Mérienne *et al.*[17] is notable for their use of near-real-time processing on a graphics processing unit to rapidly reduce the data and compute spectra and cross-correlations.

This work uses polymer/ceramic PSP with PtTFPP on a turret model at a Mach number of 0.33. The basic structure of the turret model (see Figure 2) is a hemispherical dome mounted on a cylindrical post of the same diameter. The flow over this basic structure is known to be highly unsteady, with complex interactions between the horseshoe vortex and the separated wake.[18] Intricate details of the model such as the gaps, the 'smile', and the flat window (Figure 2) are expected to introduce further complexity into the flow. Thus, it is of interest to study the unsteady surface pressure distribution to understand these complex fluid interactions. The frequencies of the wake dynamics are expected to be on the order of 100 Hz, with higher harmonics also present. The response of fast PSP, flat to at least 6 kHz, is more than sufficient for the current study. The fluorescent intensity of the paint was recorded from three high-speed cameras, providing for a nearly-complete measurement of local instantaneous pressure over the exterior surface of the turret model. Since high-speed imaging was used, transient pressure features are clearly visible and provide insight into the complex wake dynamics of the turret model.[18] In this paper, only a small collection of turret configurations will be presented. The primary focus of this paper is on the development and implementation of the measurement technique, illustrated by the analysis of this subset of test cases. Other measured cases are presented and analyzed in detail by Gordeyev *et al.*[19] Also, knowing the unsteady pressure field, it is possible to compute unsteady force components acting on the turret, which is addressed by De Lucca *et al.* in a separate paper.[20]
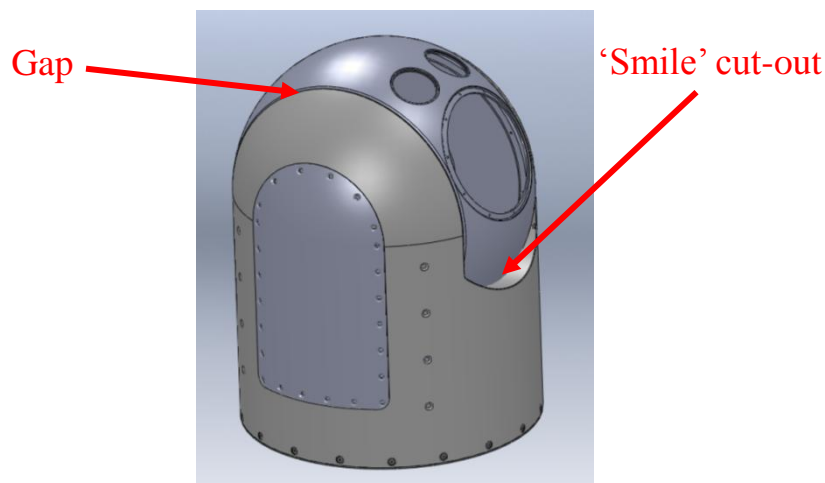

Figure 2: Turret model.

II. Experimental Methodology

The tested turret model (Figure 2), measuring 0.3-m (1-ft) in diameter and 0.26-m (0.87-ft) in height, is an exact replica of turret shell used on the Airborne Aero-Optics Laboratory (AAOL) for aero-optical flight tests.[21] The turret has a rotating center portion, allowing changes to the elevation angle, while the whole turret assembly was able to rotate to any azimuthal angle. The turret had several realistic features such as gaps between the rotating portion of the turret and trunnions, as well as cut-outs, or 'smiles', on both sides of the stationary portion of the turret.

The turret was tested in the recirculating wind tunnel at the White Field facility at the University of Notre Dame, as shown in Figure 3. Figure 4 presents a picture and a schematic of the layout of the experimental hardware. Each side of the tunnel hosted four arrays of ultraviolet LEDs in a 2-by-2 grid, providing continuous excitation while the cameras were being exposed. Two high-speed cameras, labeled the far ("port" side) and the near ("starboard" side) cameras, were positioned on either side of the tunnel, viewing the downstream sides of the turret at an oblique angle. A third high-speed camera, labeled the top camera, was placed atop the tunnel, viewing the front and top of the turret. Each of the high-speed cameras was operated at a frame rate of 2 kHz, a rate that was a tradeoff between available light per frame and the time scale of the expected pressure fluctuations. Relevant details about each camera are given in Table 1. Because of the optical configuration of the illumination LEDs, the sides of the model

American Institute of Aeronautics and Astronautics

had the best illumination, and the most-upwind and most-downwind points had the least. For the purposes of the discussion in this paper, cameras are named by the side of the tunnel on which they were placed, relative to the operator's bench (to the right of the diagram in Figure 4(b)). Each camera was fitted with a long-pass optical filter, ensuring that the intensity recorded was due to the fluorescence of the paint rather than reflected short-wavelength illumination.
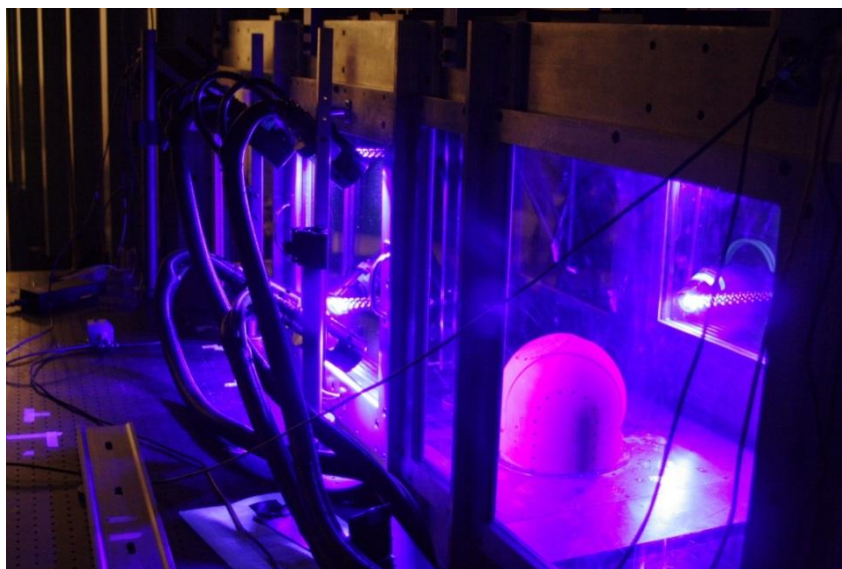

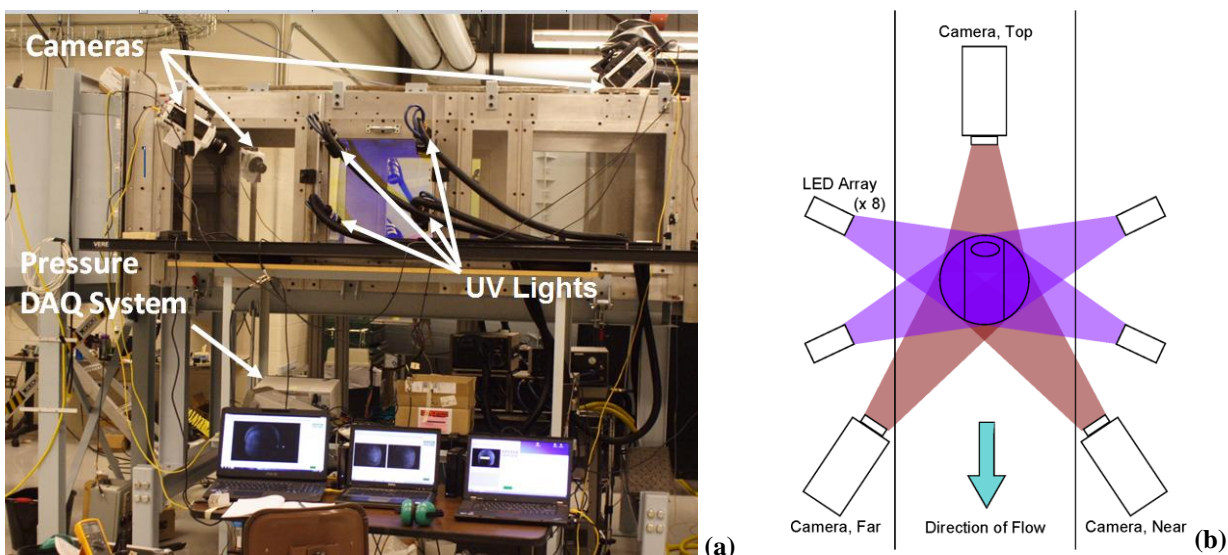**Figure 3: Turret model in the test facility, with flow from right to left.**

Figure 4: Hardware configuration: (a) Picture and (b) top-view schematic of wind tunnel.

Table 1: Camera properties.

	Far Camera	Near Camera	Top Camera
Colorspace	Grayscale	Grayscale	RGB
Resolution	1280×800	1024×768	1280×800
Frame Limit	5,477	7,000	7,000
Frames per Second	2,000	2,000	2,000

4
American Institute of Aeronautics and Astronautics

Nearly the entire surface of the model was visible within the view of at least one of the cameras. Areas of poor visibility existed at the base of the model on either side of the stagnation point, due to the elevated position of the top camera and the rearward positioning of the two side cameras. The window of the turret was visible in all three views under certain test conditions, and most of the downstream side of the model was visible from both side cameras. The turret geometric configurations tested in this work are indicated in Table 2. Each configuration includes a test with a flat window and a separate test with a conformal window. In addition, tests were performed in which either the gaps surrounding the movable center ring or both gaps and 'smiles' were covered with metal tape, presenting the flow with a smooth surface rather than a cavity. Azimuth angle was measured clockwise from the upstream direction (when viewed from above), and elevation angle was measured upward from the horizontal.

Each configuration of the model was imaged twice using the high-speed cameras for wind-off and wind-on conditions (a characteristic procedure for PSP measurements). Five hundred frames were taken with the LED arrays illuminating the surface of the model with the wind off. The elementwise mean of these frames provides a reference intensity for each pixel while averaging out frame-to-frame shot noise. Wind-on images were recorded at a rate of 2 kHz for a total record length of 5477 frames. The cameras were configured such that all three were triggered simultaneously.

The turret model was instrumented with thirteen point sensors, including eight fast-response pressure transducers and five thermocouples, shown in Figure 5. The arrangement of these sensors was intended to ensure the presence of at least one reference point in each frame of data, in order to provide for an *in situ* adjustment to the PSP data. Data acquired by these sensors, as well as the timing information for the camera synchronization, was digitally recorded. An additional pressure transducer measured the interior pressure of the turret, which was reported as an average value over the course of a run.

Table 2: Test matrix of turret positions.

		Azimuth				
		0°	90°	125°	143°	180°
Elevation	45°	×	×			×
	60°				×	
	65°		×			
	69°			×		
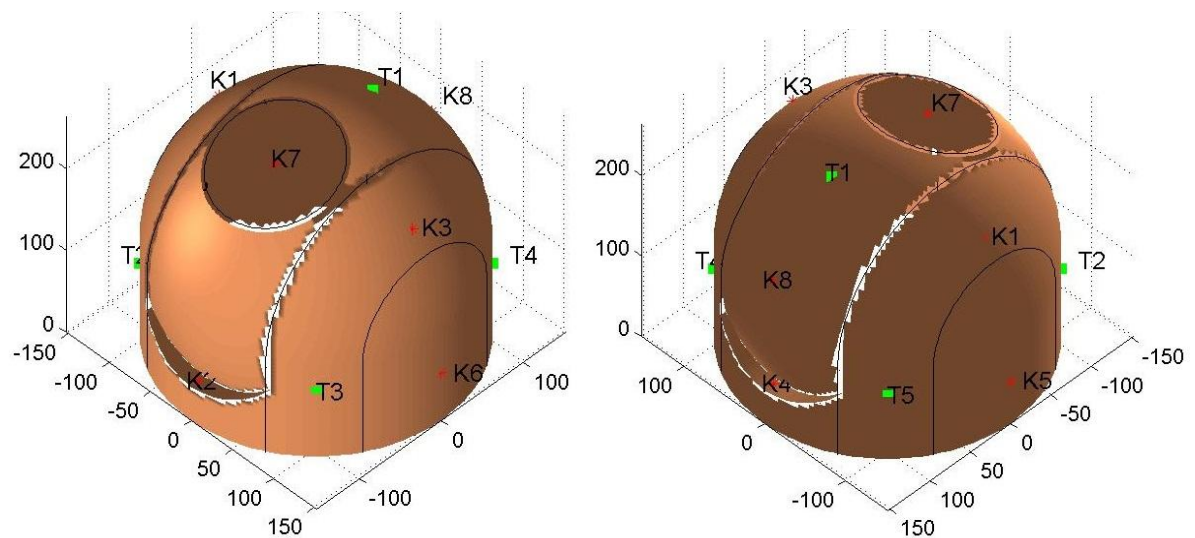
Figure 5: Locations of pressure sensors (K1-K8) and thermoprobes (T1-T5); all dimensions are in mm.

American Institute of Aeronautics and Astronautics

III. Data Reduction

A. Intensity Ratio and Image Registration

Standard practice for PSP data reduction in the radiometric mode requires the ratio of a wind-on image with a reference image at wind-off conditions (known pressure). The intensity ratio removes the effect of non-uniform illumination, paint thickness, and luminophore concentration on the indicated pressure since these effects cancel in the ratioing process. This ratio process may be described by the Stern-Volmer equation,

$$\frac{I_{ref}}{I} = A + B\frac{P}{P_{ref}},$$
(1)

where I is intensity, P is pressure, the subscript *ref* indicates wind-off reference conditions, and A and B are temperature-dependent calibration coefficients.

A proper intensity ratio requires that the model be in the exact same position and orientation in the image plane for the wind-on and wind-off conditions. This is rarely the case in wind tunnel testing due to the non-trivial applied aerodynamic loads which cause a bulk deflection of the model. Furthermore, the unsteady loading on the model in the current test causes variations of model position during the run. The top camera suffered the most from this effect, due to the predominant motion of the turret in the transverse direction. Correction was implemented by registering each frame to the silhouette of the wind-off average using a fast Fourier transform-based function with subpixel accuracy.[22] The silhouette was used as the base for registration in order to minimize the effects of noise caused by the CMOS sensors in the cameras, which can exert unwanted influence on the registration algorithm if present in both the base and instantaneous image.

B. Paint calibration

An *a priori* calibration was performed using a painted coupon placed in a pressure- and temperature-controlled calibration chamber. At each of a specified series of conditions, an image of the coupon was made, and the conditions and average intensity recorded. Reference conditions were chosen to closely approximate those of the wind-off runs, and the pressure and intensity were normalized by these reference conditions. Surface fitting was employed to provide a function returning pressure ratio as a function of intensity ratio and instantaneous temperature. The resulting surface fit was a quadratic function of intensity ratio and a linear fit of temperature,

$$\frac{P}{P_{ref}} = C_0 + C_1\frac{I_{ref}}{I} + C_2\left(\frac{I_{ref}}{I}\right)^2 + C_3 T + C_4 \frac{I_{ref}}{I}T.$$
(2)

An *in situ* adjustment was performed in order to correct for erroneous bulk shifts of the paint's indicated pressure. Such discrepancies can potentially be caused by phenomena such as temperature drift or photodegradation of the paint. The *in situ* adjustment is in effect a correction to the pressure calculations to ensure the best possible match with the known data from the point sensors. Each sensor is visible in one or more camera's views. To perform this adjustment, a sample of the pressure calculated from the *a priori* calibration as described above was taken for each pressure sensor in each camera view. The shape of this sample in the plane of the frame was a thin annulus centered on the sensor, which avoided sampling the unpainted sensor or its immediate surroundings, where the sensor mount in some cases caused local temperature variations which affected pressure measurements. The mean pressure reported in this sample was averaged over the course of the run to obtain an uncorrected datum, and the data reported by the sensor was averaged over the course of the run to obtain the true pressure. Because the number of sensors in each view was not constant, the average difference between the uncorrected and known values for each camera view was computed, and the pressure data were corrected by incrementing or decrementing by this difference. In some cases, the sensor was placed in such a way that it was not possible to center an annulus of sufficiently large radius on the sensor, e.g. the sensor was located near the edge of the camera's view and thus only seen obliquely.

C. Data Representations

Following conversion of intensity data to pressure via the calibration, the pressure data were spatially filtered in the image plane using a 20×20 pixel edge-preserving smoothing filter. Pressure data reported in this paper is presented as a ratio of the instantaneous pressure to the mean of the local pressure. This representation isolates the pressure fluctuations, which are of primary interest in this study. The results presented here are retained in the

American Institute of Aeronautics and Astronautics

image frame of reference, while Gordeyev *et al.*[19] and De Lucca *et al.*[20] have mapped the data to a mesh of the turret model. This process is described as follows.

Integration of the pressure data to determine the loads requires a mapping of the pressure information to a mesh representation of the model. Knowing exact location of each camera, relative to the turret, it is possible to map the pressure field from 2-D images onto the 3-D surface of the turret, using the Perspective Transformation Matrix (PTM) technique.[23-25] Schematically, the perspective projection is shown in Figure 6.
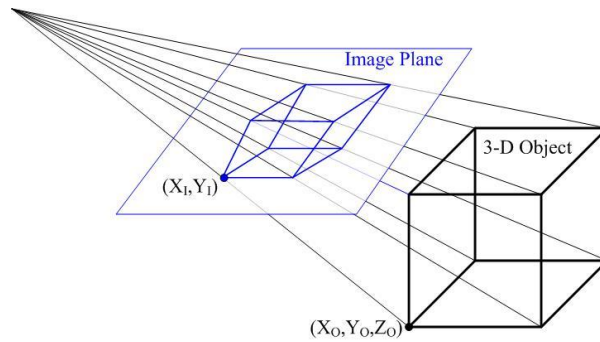
Figure 6. Schematic of perspective projection.

The perspective transformation allows one to compute the (X_I, Y_I)-location of the image point, if a 3-D coordinate of the object point, (X_O, Y_O, Z_O), is given, as,

$$\begin{bmatrix} a \\ b \\ w \end{bmatrix} = M * \begin{bmatrix} X_O \\ Y_O \\ Z_O \\ 1 \end{bmatrix}, \quad X_I = a/w, \quad Y_I = b/w, \tag{3}$$

where M is the 3×4 Perspective Transformation Matrix, defined by the camera location and orientation angles. As accurate measurements of the camera orientation are difficult in practice, an alternative way to obtain the PTM is to take images of several non-coplanar points with known 3-D coordinates. After extracting the 2-D locations of the points from the image, a PTM can be reconstructed using a least-square estimation.[24] The advantage of this method is that it does not require explicit knowledge of the camera's location and orientation.

To accomplish this procedure, at the end of the PSP tests the turret was replaced with a calibration mask, which consisted of a series of small printed dots at known locations. The mask was placed horizontally and then vertically, with images of the mask recorded by all three cameras for each case. After extracting the 2-D locations of the dots from the images, a PTM was calculated for each camera.

The entire turret surface was approximated with a relatively dense grid, shown in Figure 7, middle plots. Then the turret surface was split into three regions to provide a unique mapping between the turret surface and the corresponding cameras' images. Using the PTM for each camera, an image point corresponding to every grid point on the surface of turret was calculated. After instantaneous pressure values at every grid point on the surface of the turret in each region were computed, the full surface pressure field was reconstructed, using weighing functions, shown in Figure 7, middle plots, to "blend" data from the different cameras. An example of the final 3-D reconstruction is shown in Figure 7, where individual 2-D pressure fields, shown in the top row, were projected onto the 3-D turret surface, shown in the bottom plot of Figure 7.

As discussed in the previous section, the near and far cameras were monochromatic, while the top camera was an RGB color camera. In order to capture different colors, the camera utilizes the Bayer color filter mask on the pixel array of the image sensor, where each two-by-two cell contains two green, one blue, and one red filter. As an unintended consequence, the color camera measured the intensity of the PSP emission (in the red spectrum) on staggered grids with a ½ × ½ loss of spatial resolution. A second issue with the color camera was that a combination of the staggered color grid and filters reduced an overall amount of intensity of the image, from 1000-2000 counts for the monochromatic camera down to 100-200 counts for the color camera (a factor of 5 reduction). As image data are discrete both in space and in intensity values, this decrease in an overall intensity of the image resulted in an increased discretization error, up to 4-7% of the dynamic pressure, *q,* versus 0.7-1.5% of *q* for the monochromatic cameras. The top camera measured the region in the front of the turret, where pressure fluctuations, measured by

unsteady pressure sensors, were found to be approximately 1-2% of the dynamic pressure. The combination of greatly reduced intensity and 75% lower spatial resolution led to very low signal-to-noise ratios for the top camera images. After various attempts to reduce the noise present in top camera by applying different filters, the resulting signal-to-noise was still very low and data from the top camera was ultimately excluded from the present analysis.

Thus, results from only two of the cameras were used to reconstruct the spatially- and temporally-resolved pressure field over the downstream half of the turret surface. This representation of the data was employed by Gordeyev et al.[19] and De Lucca et al.[20] in further analysis of the PSP results.
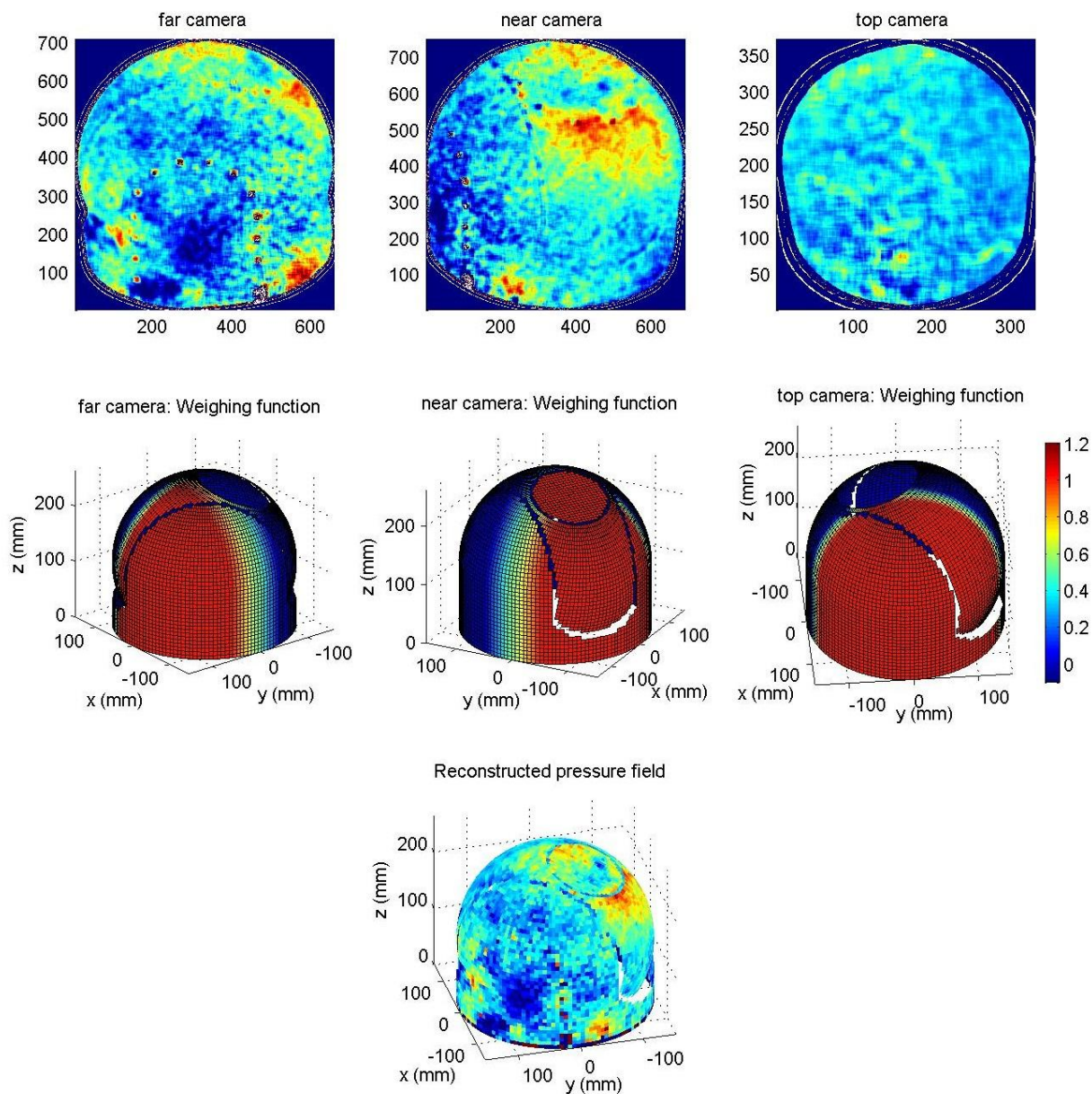
Figure 7: Top: Individual Frames from cameras. Middle: corresponding weighting functions. Bottom: reconstructed instantaneous pressure field on the surface of the turret. Flow is oriented along the x-axis from positive to negative values.

IV. Results and Discussion

The time-varying pressure distributions over the surface of the turret were determined using high-speed digital imaging of the model coated with porous pressure-sensitive paint. As mentioned in the introduction, the main purpose of this paper is to describe the measurement technique (PSP) applied to this investigation, and to highlight the various data analysis techniques that may be used with this spatially- and temporally-resolved data set. The effect of altering the azimuth and elevation angles on the pressure distribution and features is examined. Some of the geometric effects are discussed herein, while a more exhaustive treatment is given by Gordeyev *et al.*[19] and De Lucca *et al.*[20] The following results are grouped by discussion of prominent flow features, preceded by a description of the analysis techniques used.

A. Analysis techniques

Based on the high-intensity illumination and high-speed cameras, PSP provided time-resolved pressures over the entire model. Three separate cameras recorded the data, which could then be mapped to a three-dimensional mesh (see Figure 7). The following results, however, focus on the two cameras viewing the aft portion of the model (the "far" and "near" cameras seen in Figure 4). These views illustrate most of the predominant pressure features on the model. Since unsteady pressure is the key quantity of interest here, the results will be presented as normalized pressure fluctuations (P'/P_{mean}). In an effort to reduce the impact of shot noise, the results have been filtered with a 20×20 pixel edge-preserving smoothing filter. As it was shown in the companion paper[19], applying proper orthogonal decomposition (POD) to the unsteady pressure data results in further suppression of the noise.

With such a large data set, it can be difficult to manipulate the results to extract meaningful insight. Data animations of the pressure fluctuations are helpful, but not accessible for a written paper. A map of the root-mean-square pressure can provide an indication of regions of high pressure fluctuations. Pressure time histories for individual pixels (virtual pressure taps) may be plotted and compared, with cross-correlations performed between different locations on the model surface. Furthermore, spatial representations of spectral content are helpful for visualizing flow structures. A power spectrum based on the FFT can be calculated for the pressure time history at each pixel location. The spectral energy may be integrated over bands and presented as separate maps for visualization of the spatial structure of spectral energy.[12-14] The pressure data can also be represented via proper orthogonal decomposition (POD), which is addressed by the companion papers to this one.[19,20]

B. Pressure features
1. Longitudinal pressure fluctuations at the turret base

The predominant fluctuating pressure on the turret is represented by longitudinal (vertical) pressure features on either side of the model. These can be seen in the instantaneous pressure images in Figure 8 by the high and low pressure regions on the left and right sides of the model, respectively. The fluctuations are present for every geometrical configuration of the turret (varying in strength), with the 0°/45° (azimuth/elevation) flat-window case being shown here. This configuration has the flat window oriented upwards at 45° and pointing directly into the freestream. Furthermore, the 'smile' is symmetric about the freestream velocity direction.

The longitudinal fluctuating pressure regions observed in Figure 8 likely correspond with the movement of the separation line of the flow around the turret. In the instance shown in Figure 8, the pressure features indicate a delayed separation on the far side of the model and earlier separation on the near side. These inferences are supported by the fact that the pressure fluctuations are 180° out of phase with one another, as illustrated in the representative pressure time histories shown in Figure 9. These virtual taps were sampled from the larger data set at a small region of interest near the edge of the turret in the far and near camera fields of view. The cross-correlation of these two simultaneously-acquired signals (Figure 10) verifies that they are 180° out of phase. The power spectra associated with these two pressure features are shown in Figure 11. The predominant frequency at 71.3 Hz in both spectra corresponds to a Strouhal number of 0.19. Higher-frequency components visible in the spectra are likely due to smaller-scale flow structures originating at the 'smile' on the model and convecting downstream (to be discussed later in this paper).

American Institute of Aeronautics and Astronautics
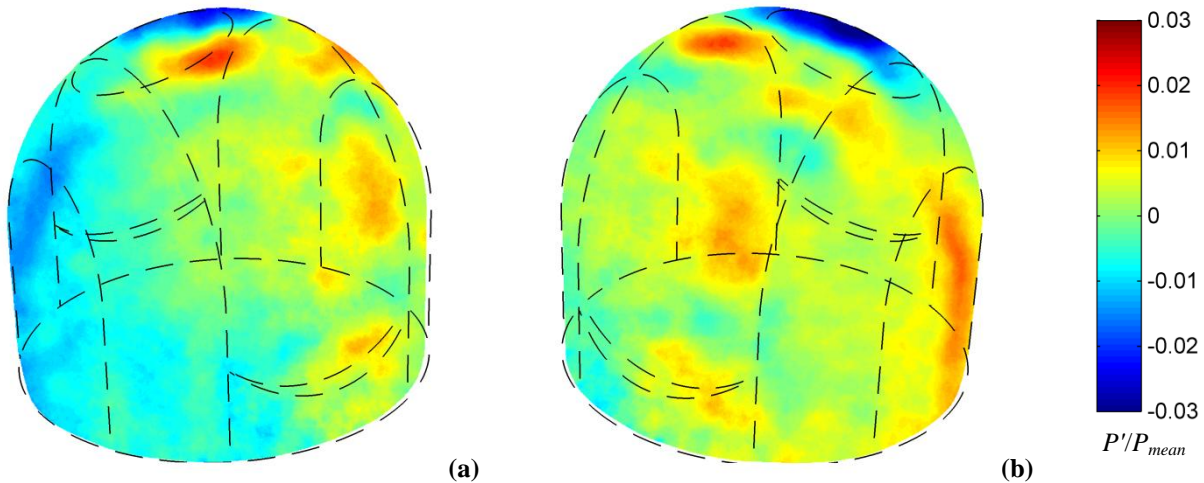
(a)   **(b)**

Figure 8: Instantaneous pressure fluctuations viewed by the far (a) and near (b) cameras for the turret at 0°/45°. Note the low-pressure longitudinal feature on the left side of the far image (a) and the simultaneous high-pressure feature on the right side of the near image (b).
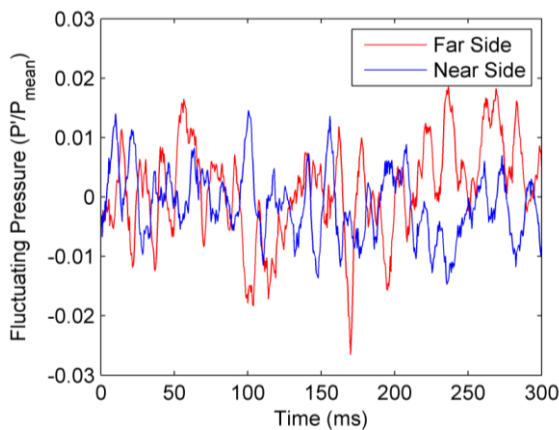

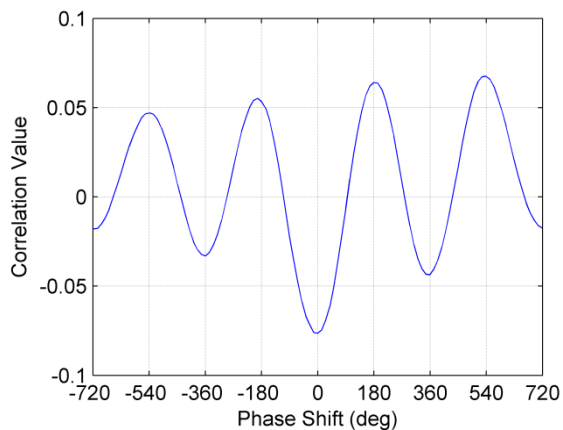**Figure 9: Sample time history of pressure fluctuations.**

Figure 10: Cross-correlation of the far- and near-side pressure signals shown in Figure 9, indicating a strong correlation with 180° phase shift.
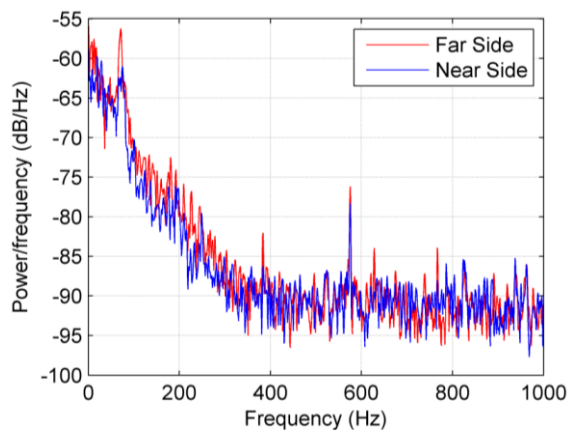
Figure 11: Power spectra of the far- and near-side pressure signals shown in Figure 9.

10
American Institute of Aeronautics and Astronautics

2. High-frequency fluctuations at the turret apex

At the apex of the turret there exist smaller-scale pressure features that are much higher in frequency, as shown in Figure 12. In fact, the apparent convective speed of these pressure features is so high that the frame rate of the cameras (2 kHz) is not quite sufficient to capture the complete temporal evolution of these features. The spatial structure and orientation of these pressure fluctuations is consistent with the expected pressure imprint of a separated shear layer originating from geometrical discontinuity near the trailing edge of the window oriented at 45°. This shear layer appears to interact with the adjacent longitudinal separation lines in a quasi-periodic manner.

Maps of the root-mean-square of the normalized pressure fluctuations (Figure 13) clearly show the locations of both the longitudinal pressure fluctuations and the high-frequency fluctuations at the apex. Regions of elevated rms are also visible adjacent to the downstream 'smile' near the base of the turret.

3. Local vortices

Certain geometrical configurations of the turret exhibited small, unsteady regions of low pressure. For example, for the 125°/69° (azimuth/elevation) flat window configuration (Figure 14), a low-pressure region exists just below the window with an accompanying high-pressure region present on the window face. This is likely due to the formation of an unsteady vortex in this region. The vortex moves about the surface of the flat window in a chaotic manner, and is not always present. The image sequence in Figure 14 is typical of when the vortex is present in the vicinity of the window. Note that this significant pressure feature is small and localized, which would make it difficult to resolve this feature with conventional transducers.

Another example of small-scale vortex formation on the surface is shown in Figure 15, also for the 125°/69° flat window case. In this instance, there are two small-scale low pressure regions in close proximity, which are likely due to vortices interacting with the surface. The two vortices (labeled "A" and "B" in Figure 15) exhibit interesting interactions with one another on a very short time scale. When the two are in proximity, the two move in a counter-clockwise fashion with vortex B convecting rapidly upstream and vortex A moving downstream. This behavior is indicative of both vortices having vorticity of the same sense – if both have positive streamwise vorticity then their mutual induction will force vortex motion in this counter-clockwise fashion. The origin of the vortices could be the secondary vortex (formed due to the presence of the necklace vortex), or possibly at the edge of the 'smile' as flow spills over the lip of the 'smile'. In both cases, the sense of the vorticity is expected to be positive streamwise, indicating that the observed interactions could be attributed to the secondary vortex and a 'smile' vortex.

The locations of both of these flow features – the unsteady vortices near the window and those at the base of the turret – are clearly visible in the root-mean-square pressure fluctuation maps (Figure 16). The precise location of the window fluctuations is identified by elevated rms over a small portion of the window (denoted by the arrow in Figure 16(b)), while the region of interacting vortices is visible in Figure 16(a).
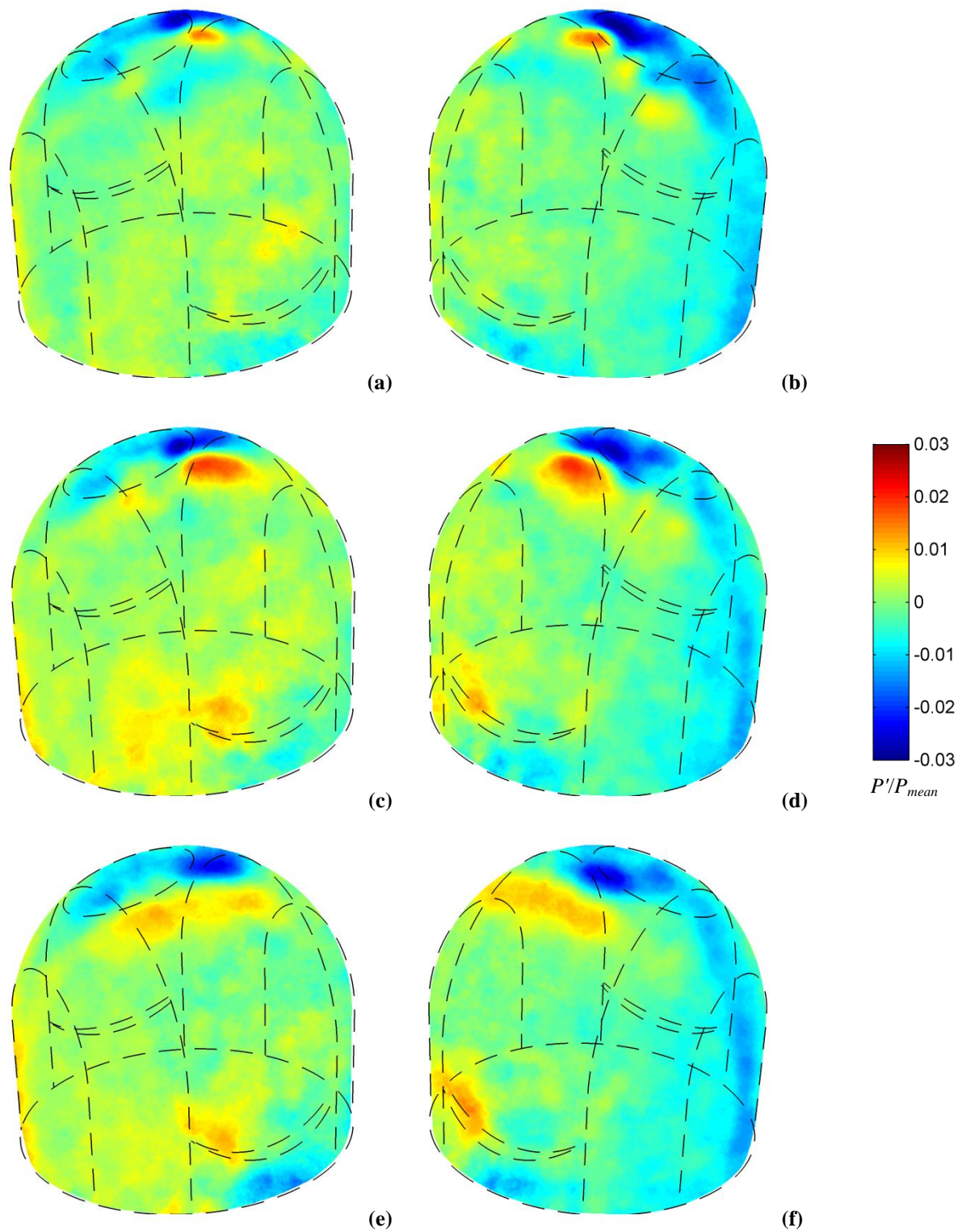
11
American Institute of Aeronautics and Astronautics

Figure 12: Instantaneous pressure fluctuations viewed by the far (a,c,e) and near (b,d,f) cameras for the turret at 0°/45°, with each image pair separated by 500 ms in time. Note the convection of the alternating low/high pressure region at the apex of the turret.
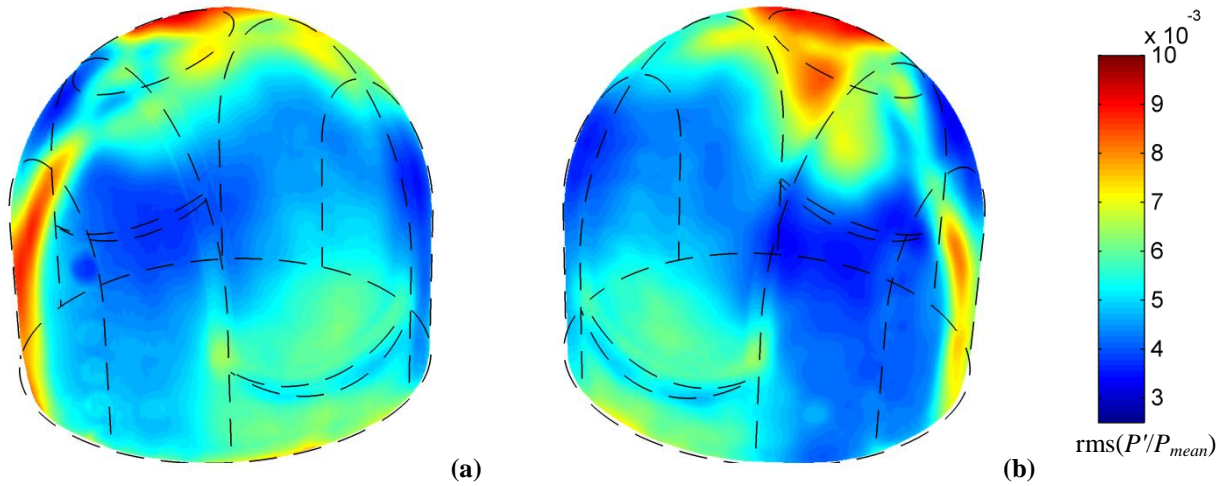
Figure 13: Rms pressure fluctuations (P'/P_{mean}) for the far (a) and near (b) camera views of the flat-window turret at 0°/45°.
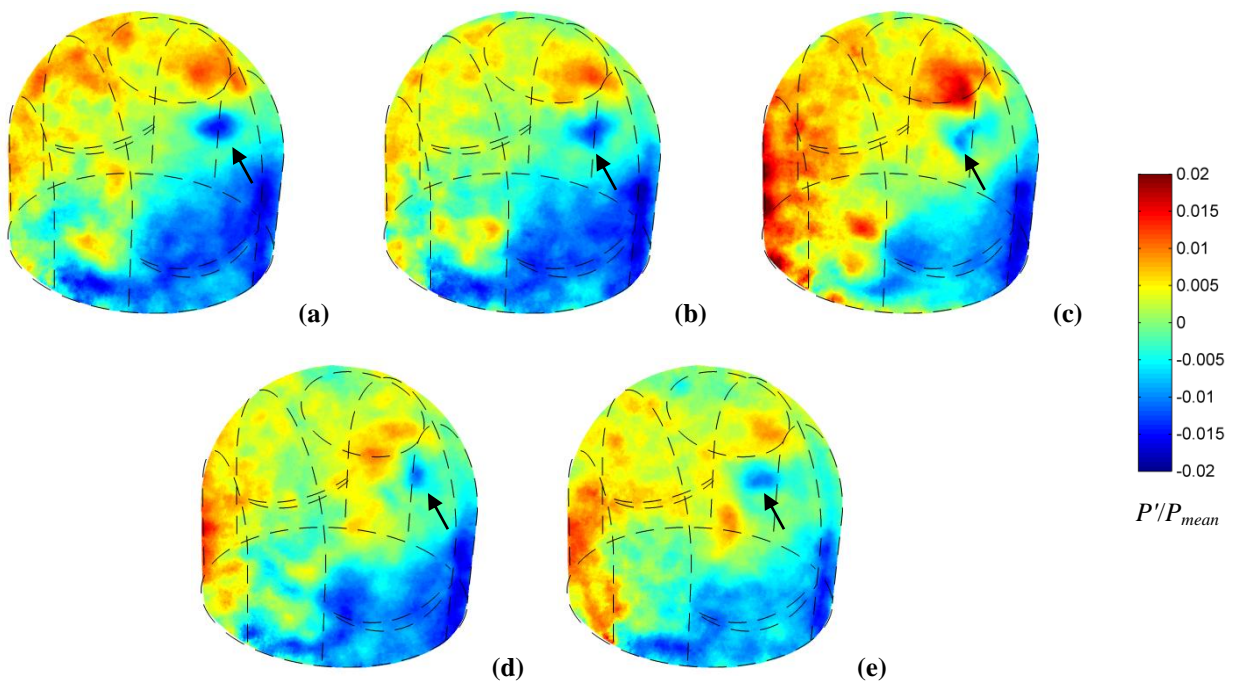

Figure 14: Progression of low-pressure region associated with vortex formation on the window of the 125°/69° flat window case (near camera) with 500 ms separating each image from (a) to (e).

13
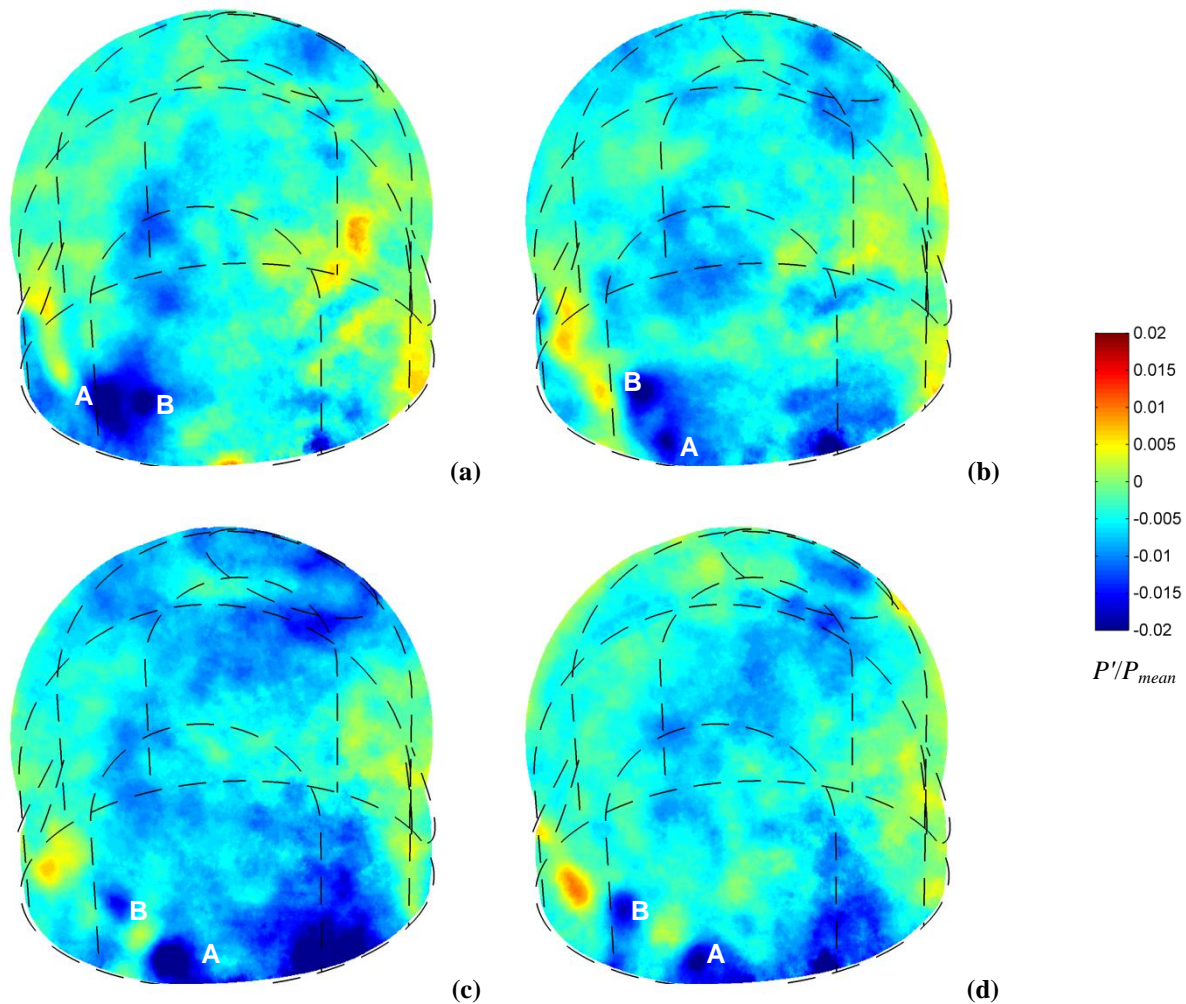American Institute of Aeronautics and Astronautics

Figure 15: Interacting vortices near the base of the turret in the 125°/69° flat window case (far camera) with 500 ms separating each image from (a) to (d). Two interacting vortices are labeled "A" and "B".
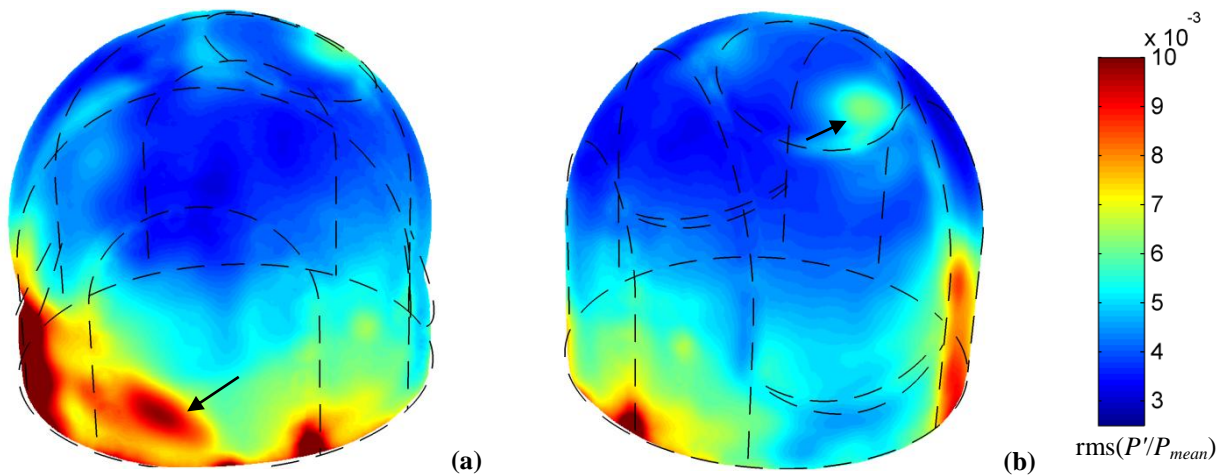

Figure 16: Rms pressure fluctuations (P'/P_{mean}) for the far (a) and near (b) camera views of the flat-window turret at 125°/69°.

14

American Institute of Aeronautics and Astronautics

V.   Conclusion

The time-varying pressure distribution over the surface of a turret was determined using high-speed digital imaging of a model coated with fast-response pressure-sensitive paint. The PSP, sampled at 2 kHz, provided detailed spatially- and temporally-resolved pressure information over much of the model surface. This rich data set enables a detailed study of the flow features resulting from various geometric configurations and turret orientations. The focus of this paper has been on the details of implementation of the measurement technique and a brief review of various analysis methods. Several predominant flow features of the turret were discussed primarily to illustrate the capabilities of the fast-response PSP technique. The key advantage of PSP is its high spatial resolution; PSP is able to resolve small-scale pressure features that move on the surface of the model. Conventional instrumentation, such as an array of small unsteady pressure sensors, would miss recording these pressure features and could lead to erroneous conclusions about the fluid dynamics. The time-resolved capabilities of PSP are also highlighted, with pressure features of at least several hundred Hz recorded in this study. Two companion papers focus on a more in-depth analysis and interpretation of the pressure results[19] and integration of the pressure data to determine the time-resolved loading on the turret for flight testing.[20] Future work with high-speed imaging of PSP on the turret will incorporate three improvements to the data acquisition process: only gray scale cameras will be used for imaging (to avoid the low intensity and poor resolution of the color camera), the optical transmission characteristics of the tunnel windows will be optimized for the excitation light, and a higher sample rate will be employed for capturing the full range of spectral content.

Acknowledgments

References

1. Liu, T. and Sullivan, J. P., *Pressure and Temperature Sensitive Paints*, Springer, Berlin, 2005.

2. Bell, J. H., Schairer, E. T., Hand, L. A., and Mehta, R. D., "Surface Pressure Measurements Using Luminescent Coatings," *Annual Review of Fluid Mechanics*, Vol. 33, 2001.

3. Gregory, J.W., Sakaue, H., Liu, T., and Sullivan, J. P., "Fast Pressure-Sensitive Paints for Flow and Acoustic Diagnostics," *Annual Review of Fluid Mechanics*, Vol. 46, 2014.

4. Gregory, J. W., Asai, K., Kameda, M., Liu, T., and Sullivan, J. P., "A Review of Pressure-Sensitive Paint for High-Speed and Unsteady Aerodynamics," *Proceedings of the Institution of Mechanical Engineers, Part G: Journal of Aerospace Engineering,* Vol. 222, No. 2, 2008, pp. 249-290.

5. Sugimoto, T., Kitashima, S., Numata, D., Nagai, H., and Asai, K., "Characterization of Frequency Response of Pressure-Sensitive Paints," AIAA 2012-1185, 50th AIAA Aerospace Sciences Meeting and Exhibit, Nashville, TN, 2012.

6. Peng, D., Jensen, C. D., Juliano, T. J., Gregory, J. W., Crafton, J., Palluconi, S., and Liu, T., "Temperature-Compensated Fast Pressure-Sensitive Paint," accepted for publication in *AIAA Journal*, 2013.

7. McMullen, R. D., Huynh, D., Gregory, J. W., and Crafton, J. W., "Dynamic Response Calibrations of Pressure-Sensitive Paint," 43rd AIAA Fluid Dynamics Conference, San Diego, CA, 24-27 June 2013.

8. Gregory, J. W., Sullivan, J. P., Wanis, S. S., and Komerath, N. M., "Pressure-sensitive paint as a distributed optical microphone array," *Journal of the Acoustical Society of America*, Vol. 119, No. 1, 2006, pp. 251-261.

9. Disotell, K. J. and Gregory, J. W., "Measurement of transient acoustic fields using a single-shot pressure-sensitive paint system," *Review of Scientific Instruments*, Vol. 82, No. 7, 2011, p. 075112.

10. Fang, S., Disotell, K. J., Long, S. R., Gregory, J. W., Semmelmayer, F. C., and Guyton, R. W., "Application of Fast-Responding Pressure-Sensitive Paint to a Hemispherical Dome in Unsteady Transonic Flow," *Experiments in Fluids*, Vol. 50, No. 6, 2011, pp. 1495-1505.

11. Fang, S., Long, S. R., Disotell, K. J., Gregory, J. W., Semmelmayer, F. C., and Guyton, R. W., "Comparison of Unsteady Pressure-Sensitive Paint Measurement Techniques," *AIAA Journal*, Vol. 50, No. 1, 2012, pp. 109-122.

12. Nakakita, K., "Unsteady pressure distribution measurement around 2D-cylinders using pressure-sensitive paint," AIAA 2007-3819, 25th AIAA Applied Aerodynamics Conference, Miami, FL, 2007.

13. Nakakita, K., "Unsteady pressure measurement on NACA0012 model using global low-speed unsteady PSP technique," AIAA 2011-3901, 41st AIAA Fluid Dynamics Conference, Honolulu, HI, 2011.

14. Crafton, J., Forlines, A., Palluconi, S., Hsu, K.-Y., Carter, C., and Gruber, M, "Investigation of transverse jet injections in a supersonic crossflow using fast responding pressure-sensitive paint," AIAA 2011-3522, 29th AIAA Applied Aerodynamics Conference, Honolulu, HI, 2011.

15. Nakakita, K., Takama, Y., Imagawa, K., and Kato, H., "Unsteady PSP measurement of transonic unsteady flow field around a rocket fairing model," AIAA 2012-2758, 28th AIAA Aerodynamic Measurement Technology, Ground Testing, and Flight Testing Conference, New Orleans, LA, 2012.

16. Nakakita, K. and Arizono, H., "Visualization of unsteady pressure behavior of transonic flutter using pressure-sensitive paint measurement," AIAA 2009-3847, 27th AIAA Applied Aerodynamics Conference, San Antonio, TX, 2009.

17. Mérienne, M. C., Le Sant, Y., Lebrun, F., Deleglise, B., and Sonnet, D, "Transonic buffeting investigation using unsteady pressure-sensitive-paint in a large wind tunnel," AIAA 2013-1136, 51st AIAA Aerospace Sciences Meeting, Grapevine, TX, 2013.

18. Gordeyev, S. and Jumper, E., "Fluid dynamics and aero-optics of turrets," *Progress in Aerospace Sciences*, Vol. 46, 2010, pp. 388-400.

19. Gordeyev, S., De Lucca, N., Jumper, E., Hird, K., Juliano, T. J., Gregory, J. W., Thordahl J., and Wittich, D. J., "The Comparison of Unsteady Pressure over Flat- and Conformal-Window Turrets using Pressure Sensitive Paint," 43rd AIAA Fluid Dynamics Conference, San Diego, CA, 24-27 June 2013, San Diego, CA, 24-27 June 2013.

20. De Lucca, N., Gordeyev, S., Jumper, E., Hird, K., Juliano, T. J., Gregory, J. W., Thordahl J., and Wittich, D. J., "The Estimation of the Unsteady Force Applied to a Turret in Flight," 43rd AIAA Fluid Dynamics Conference, San Diego, CA, 24-27 June 2013.

21. Jumper, E. J., Zenk, M., Gordeyev, S., Cavalieri, D., and Whiteley, M. R., "Airborne Aero-Optics Laboratory," *Journal of Optical Engineering*, Vol. 52, No. 7, 2013, p. 071408.

22. Guizar-Sicairos, M., Thurman, S. T., and Fienup, J. R., "Efficient subpixel image registration algorithms," *Optics Letters*, Vol. 33, No. 2, 2008, pp. 156-158.

23. Carlbom, I. and Paciorek, J., "Planar Geometric Projections and Viewing Transformations," *ACM Computing Surveys*, Vol. 10, No. 4, 1978, pp. 465–502.

24. Haralick, R. M., "Using Perspective Transformations in Scene Analysis," *Computer Graphics and Image Processing*, Vol. 13, 1980, pp. 191-221.

25. Tan, T. N., Sullivan, G. D., and Baker, K. D., "On computing the perspective transformation matrix and camera parameters," *Proceedings of the 4th British Machine Vision Conference*, Surrey, England, 1993, pp. 125–134.